miR-328a-3p stimulates endothelial cell migration and angiogenesis

Sailing Chen
 Nantong University Qixiu Campus

Yunsong zhang
 Nantong University Qixiu Campus

Xiaodong Cai
 Nantong University Qixiu Campus

Sheng Yi
 Nantong University Qixiu Campus

Xinghui Wang (✉ xhwang@ntu.edu.cn)
 Nantong Uniwersity Qixiu Campus   https://orcid.org/0000-0003-3938-1253

Research

Abstract

Background

Endothelial cells play important biological roles after peripheral nerve injury by forming blood vessels within the nerve gap after peripheral nerve injury and guiding Schwann cell migration. microRNAs (miRNAs) affect cellular behavior and regulate a wide variety of physiological and pathological activities, including peripheral nerve regeneration. Emerging studies identified the essential roles of miRNAs on the phenotype modulation of Schwann cells while the effects of miRNAs on endothelial cells were not well investigated. miR-328a-3p was differentially expressed in peripheral nerve stumps after nerve injury. This study aimed to identify the biological effects of miR-328a-3p on human umbilical vein endothelial cells (HUVECs).

Methods

Here, the biological functions of miR-328a-3p on endothelial cells were determined by transfecting cultured human umbilical vein endothelial cells (HUVECs) with miR-328a-3p mimic or inhibitor. Heatmaps of lncRNAs and mRNAs were generated using meV software according to previous obtained sequencing data of sciatic nerve stumps at 0, 1, 4, 7, and 14 days after nerve crush injury.

Results

Transfection with miR-328a-3p mimic led to slightly decreased HUVEC proliferation and robustly increased HUVEC migration and tubulogenesis while transfection with miR-328a-3p mimic led to opposite observations. Bioinformatic analysis further discovered potential regulators and effectors of miR-328a-3p and constructed a miR-328a-3p-centered competing endogenous RNA (ceRNA) network.

Conclusions

Collectively, our present study demonstrated that dysregulated miR-328a-3p after peripheral nerve injury might affect the migration and angiogenesis of endothelial cells and contribute to peripheral nerve regeneration.

Trial registration:

The rats were obtained from the Experimental Animal Center of Nantong University (Animal licenses No. SCXK [Su] 2014-0001 and SYXK [Su] 2012-0031).

Background

Endothelial cells are highly plastic cells that can rapidly switch to an activated state to mediate angiogenesis during wound healing (1, 2). Formed blood vessels supply oxygen and nutrients, remove wastes, and contribute to the regeneration of various tissues and organs (3). Considering the importance of blood supply, vascularization is regarded as an essential factor during the fabrication and construction of tissue engineered products (4–6).

Angiogenesis is also very critical for the regeneration of injured peripheral nerves. Following peripheral nerve injury, polarized blood vessel formation within the bridge will guide the migration of Schwann cells towards and across the injured site and encourage axon elongation and nerve repair (7). In tissue engineered nerve grafts, sufficient angiogenesis benefits cell survival, promotes cell integration with biomaterials, provides a favorable nutritional microenvironment, and improves the regeneration and functional recovery of injured nerves (8, 9). Therefore, investigating certain approaches to modulate the phenotype of endothelial cells and to advance angiogenesis after peripheral nerve injury is of great theoretical and practical implications.

microRNAs (miRNAs) are small single-strand non-coding RNAs with about 22 nucleotides in length. miRNAs bind to their target mRNAs, induce mRNA degradation and/or translational repression, and negatively regulate their target mRNAs (10, 11). A large number of miRNAs were identified to be differentially expressed in the injured peripheral nerve stumps after nerve injury (12). Differentially expressed miRNAs might affect the proliferation, migration, and/or remyelination of Schwann cells and regulate nerve regeneration process (13). However, in spite of the essential roles of endothelial cells during peripheral nerve regeneration, the regulatory effects of miRNAs on endothelial cells, as compared with Schwann cells, remain largely unknown.

miR-328 has been involved in numerous biological activities, such as cellular apoptosis (14), brown adipose tissue differentiation (15), and glucose uptake (16). Emerging studies have associated miR-328 with numerous diseases, including leukemic blasts (17), atrial fibrillation (18, 19), intervertebral disc degeneration (20), and hepatocellular carcinoma (21). Dysregulated miR-328 was also observed in prion induced neurodegeneration (22), implying that miR-328 might play important roles in nervous system diseases. Moreover, miRNA sequencing data of rat sciatic nerve stumps after nerve transection showed that miR-328 expression was altered after peripheral nerve injury (12), suggesting that miR-328 might be essential for peripheral nerve injury and regeneration.

miR-328a-3p was previously named as miR-328 or miR-328 according to miRbase (http://mirbase.org/). Therefore, in the current study, we examined the biological effects of miR-328a-3p on human umbilical vein endothelial cells (HUVECs). Potential upstream long non-coding RNAs (lncRNAs) and downstream target mRNAs of miR-328a-3p were bioinformatically analyzed to reveal the regulatory cascade of miR-328a-3p after peripheral nerve injury.

Materials And Methods

Cell culture

HUVECs were seeded onto cell culture flasks (Corning, Coring, NY, USA) and grown in complete medium (endothelial cell medium (ECM; Sciencell, San Diego, California, USA) supplemented with 5% heat-inactivated fetal bovine serum (FBS; Sciencell), 1% endothelial cell growth supplement (ECGS; Sciencell), and 1% penicillin and streptomycin (Invitrogen, Carlsbad, CA, USA)) at 37°C and 5% CO_2 in a humidified incubator.

Cell transfection

Cultured HUVECs were transfected with a chemically synthesized miR-328a-3p mimic, mimic control, miR-328a-3p inhibitor, inhibitor control sequence (RiboBio, Guangzhou, Guangdong, China) using Lipofectamine RNAiMAX transfection reagent (Invitrogen) according to the manufacturer's instructions. The sequences of miR-328a-3p mimic were 5'-CUGGCCCUCUCUGCCCUUCCGU-3' and 3'-ACGGAAGGGCAGAGAGGGCCAG-5', the sequence of miR-328a-3p inhibitor was 5'-ACGGAAGGGCAGAGAGGGCCAG-3', and the sequences of non-targeting negative controls were random sequences. HUVECs were transfected for 48 hours prior to functional investigations.

Real-time RT-PCR

Total RNA was isolated from cultured HUVECs, reverse transcribed to cDNA using the TaqMan MicroRNA Reverse Transcription Kit (Applied Biosystems, Foster City, CA, USA), and subjected to RNA amplification using the QuantiNova SYBR Green PCR Kit (Qiagen) on an Applied Biosystems StepOne real-time PCR system. Bulge-loop^{TM} miRNA qRT-PCR Primer Sets (one RT primer and a pair of qPCR primers for each set) specific for miR-328a-3p was designed by RiboBio. The abundance of miR-328a-3p in HUVECs was compared with the internal control U6 and the quantification of miR-328a-3p was determined using the ΔΔCt method.

EdU proliferation assay

HUVECs were seeded onto cell culture plates pre-coated with poly-L-lysine, exposed with 5-ethynyl-2'-deoxyuridine (EdU) for 24 hours, and fixed with 4% paraformaldehyde. Cell proliferation was determined by using a Cell-Light EdU DNA Cell Proliferation Kit (RiboBio) following manufacturer's instructions. Images were taken using a DMR fluorescence microscope (Leica Microsystems, Bensheim, Germany). The numbers of EdU-postive cells and total cells were determined by EdU and Hoechst staining. The proliferation rates of HUVECs were calculated by dividing the numbers of EdU-postive cells to the numbers of total cells.

Wound healing assay

HUVECs were seeded onto a mold chamber with a 1 mm wide insert placed on the bottom of a 6-well plate. After cell grew confluent, placed insert was removed, leaving an blank space. Images were taken using a DMR inverted microscope (Leica Microsystems) at 0 hour and 12 hours after the removal of

placed insert. Relative cleaned areas were measured at these time points using Image-Pro Plus (Media Cybernetics, Rockville, MD, USA) from randomly selected image fields.

Transswell migration assay

Transwell chambers with 8 μm pores (Costar, Cambridge, MA, USA) were applied to determine migration abilities. The upper chambers of transwell chambers were filled with HUVECs suspended in ECM medium while the lower chambers were filled with complete cell culture medium. The upper chambers were taken out after 24 hour incubation. After wiping the upper surfaces of the upper chambers and removing cells left on the upper surfaces, the bottom surfaces of these upper chambers were stained with 0.1% crystal violet to label migrated cells. Images were taken using a DMR inverted microscope (Leica Microsystems). Crystal violet was dissolved in 33% acetic acid and the optical densities (O.D.) of crystal violet were measured at 570 nm (Bio-Tek).

Matrigel tubulogenesis assay

HUVECs were seeded onto cell culture plates pre-coated with matrigel (BD Biosciences, Corning) and incubated for 6 hours to allow the formation of tubules. Images were taken using a DMR inverted microscope (Leica Microsystems). The numbers of nodes, meshes, and branches in formed tubules were quantitated using Angiogensis analyzer in the Image J software (National Institutes of Health, Bethesda, MD, USA) (23).

Bioinformatic analysis

Upstream regulatory lncRNAs of miR-328a-3p were predicted using TargetScan. Downstream target mRNAs of miR-328a-3p were predicted using miRWalk 3.0, miRranda, and MicroRNA Target Prediction Database (miRdb). Upstream lncRNAs and downstream mRNAs were linked to construct the miR-328a-3p-centered competing endogenous RNA (ceRNA). Heatmaps of lncRNAs and mRNAs were generated using meV software according to previous obtained sequencing data of sciatic nerve stumps at 0, 1, 4, 7, and 14 days after nerve crush injury (24). Sequencing data were reserved in NCBI database with the accession number PRJNA394957 (SRP113121) (25).

Statistical analysis

A student's paired two-tailed t-test was performed for statistical analysis. The calculation of p-values and the generation of graphs were made with SigmaPlot (GraphPad Prism 6.0 software, GraphPad Software, La Jolla, CA, USA).

Results

miR-328a-3p inhibited the proliferation of HUVECs

HUVECs were cultured and transfected with the mimic or inhibitor of miR-328a-3p to examine the functional effects of miR-328a-3p on endothelial cells. Efficient up- or down-regulation of miR-328a-3p from cultured HUVECs with miR-328a-3p mimic or inhibitor was confirmed by RT-PCR examination. The transfection of HUVECs with miR-328a-3p mimic significantly increased miR-328a-3p expression (Figure 1A) while the transfection of HUVECs with miR-328a-3p inhibitor significantly decreased miR-328a-3p expression (Figure 1B) as compared with their non-targeting negative controls.

HUVECs efficiently transfected with miR-328a-3p mimic or inhibitor were exposed to EdU to determine the effects of miR-328a-3p on endothelial cell proliferation. EdU incorporation assay showed that transfection with miR-328a-3p mimic transfection slightly reduced HUVEC proliferation, with an 8.56% decrease compared with the mimic control (Figure 2A). On the contrast, transfection with miR-328a-3p inhibitor transfection slightly elevated HUVEC proliferation, with a 12.65% increase compared with the inhibitor control (Figure 2B).

miR-328a-3p promoted the migration of HUVECs

HUVECs transfected with miR-328a-3p mimic or inhibitor were seeded onto insert placed mold chambers to examine cell migration abilities. Equal wide blank spaces and same sizes of cleaned area were presented after insert removal (0 hour) in both HUVECs transfected with miR-328a-3p mimic and mimic control. Obvious cell migration was detected at 12 hours after insert removal. In HUVECs transfected with mimic control, many HUVECs migrated towards the wound area and filled the blank space. About 65% of cleaned areas were left after 12 hours of insert removal and cell culture while 35% of cleaned area was covered by migrated HUVECs (Figure 3A). HUVECs transfected with miR-328a-3p mimic exhibited great migration ability and occupied a larger space. In HUVECs transfected with miR-328a-3p mimic, left cleaned areas were significantly smaller and only about 50% of cleaned areas were left at 12 hour cell culture (Figure 3A). In contrast to the decrease of relative cleaned areas observed by miR-328a-3p mimic transfection, miR-328a-3p inhibitor transfection slightly increased relative cleaned areas (Figure 3B).

In addition to wound healing assays, transwell assays was also applied to determine the effect of miR-328a-3p on HUVEC migration. Transfection with miR-328a-3p mimic increased the amount of migrated HUVECs (stained with crystal violet) to nearly 2 folds as compared with mimic control (Figure 4A) while transfection with miR-328a-3p inhibitor reduced HUVEC migration, with a 31.07% decrease as compared with inhibitor control (Figure 4B).

miR-328a-3p promoted the tubulogenesis of HUVECs

HUVECs were seeded on matrigel-coated culture plates to probe their abilities in forming capillary-like tubes. HUVECs transfected with miR-328a-3p mimic, miR-328a-3p inhibitor, and corresponding non-targeting negative controls could all form interconnecting tube networks (Figure 5A & 5B). Summarized data from skeletonized images (Figure 5C) showed that transfection with miR-328a-3p mimic largely increased the number of formed tubes, with a 55.37% increase in the number of nodes (Figure 5E), a 34.97% increase in the number of meshes (Figure 5F), and a 28.73% increase in the number of branches

(Figure 5G) as compared with mimic control. Curtailed formations of capillary-like tubes were observed in HUVECs transfected with miR-328a-3p inhibitor (Figure 5D). Transfected with miR-328a-3p inhibitor, as compared with inhibitor control, led to a 40.63% decrease in the number of nodes (Figure 5H), a 53.10% decrease in the number of meshes (Figure 5I), and a slight decrease in the number of branches (Figure 5J).

Construction of miR-328a-3p-centered ceRNA network

Upstream regulators and downstream effectors of miR-328a-3p were analyzed by bioinformatic tools. Considering that rat sciatic nerve crush injury was commonly applied as an animal model of peripheral nerve injury and gene expression profiles of rat sciatic nerve stumps were previously determined, upstream lncRNAs and downstream mRNAs of rno-miR-328a-3p were investigated. TargetScan prediction showed that a total of 5 lncRNAs, XLOC_097278, XLOC_083369, XLOC_138151, XLOC_174539, and XLOC_053870 could bind to miR-328a-3p. miRWalk 3.0, miRranda, and miRdb prediction revealed various potential target genes of miR-328a-3p. A miR-328a-3p-centered lncRNA-miRNA-mRNA network was thus constructed (Figure 6A).

Previously achieved sequencing data showed that all identified upstream lncRNAs were up-regulated in sciatic nerve stumps after nerve crush injury (Figure 6B). However, the majority of predicted potential target mRNAs were down-regulated after nerve injury while some a few mRNAs, such as Vsig4 and Prdx5, showed increased expression levels in the injured nerve stumps (Figure 6C).

Discussion

Peripheral nerve injury and repair is a complex biological process that involves the participation of various different cell types, such as Schwann cells, fibroblasts, macrophages, and endothelial cells. Following peripheral nerve injury, microRNA (miRNA)-mediated phenotype modulation of Schwann cells have been widely explored. However, the effects of miRNAs on endothelial cells, cells that play important roles on the guidance of Schwann cell migration after peripheral nerve injury, have not been well demonstrated.

Our earlier study examined the functional effects of let-7, a well-known miRNA that belongs to the most abundant miRNA family in the genome (26), on endothelial cells (27). Here, we determined the regulatory roles of miR-328a-3p, another miRNA that was demonstrated to be dysregulated in the injured peripheral nerve stumps (12). Outcomes from wound healing assay, transwell migration assay, and matrigel tubulogenesis assay, revealed that miR-328a-3p would significantly promote the migration of endothelial cells and stimulate the formation of functional capabilities. Considering that proliferating cells were variables of these assays, EdU proliferation assay was also conducted. On the contrary to the effects of miR-328a-3p on endothelial cell migration and tubulogenesis, elevated miR-328a-3p slightly decreased EdU incorporation. These results excluded the possibility that enhanced endothelial cell migration and tubulogenesis was caused by increased numbers of cells and emphasized the promoting roles of miR-328a-3p on endothelial cell migration and angiogenesis.

The functional roles of miR-328a-3p on cell migration seemed to be contradictory in various different cell types. It was reported that miR-328 could function as an anti-oncogene, repress cell migration in gastric cancer cells (28) and in osteosarcoma cells (29). On the contrary, in breast cancer cells, elevated miR-328-3p could decrease the abundances of glutamate metabotropic receptor 4 (GRM4) and counteract GRM4-induced inhibition of breast cancer cell migration and invasion (30). Notably, recent studies showed that miR-328a-3p might even lead to different cellular behaviors in endothelial cells exposed to diverse culture conditions. Under high glucose and low serum condition, the migration and tube-like structure formation of HUVECs were decreased while the expression of miR-328 was increased. Transfection high glucose and low serum-cultured HUVECs with miR-328 inhibitor would stimulate cell migration and angiogenesis (14). Another study showed that miR-328-3p would promote HUVEC migration and invasion and protect HUVECs against oxidized low-density lipoprotein induced injury (31). These conflicting observations implied that miR-328 might execute diverse functions under different microenviroment. In the current study, we examined the biological roles of miR-328a-3p of HUVECs cultured in a standardized condition. However, peripheral nerve injury generally induce a hypoxia response at the injury site (7, 32). In future studies, it would be helpful to mimic the pathological conditions of peripheral nerve injury, expose miR-328a-3p-treated HUVECs to decreased oxygen levels, and determine the modulating effects of miR-328a-3p on HUVEC phenotype under low oxygen levels.

Besides the functional investigations of miR-328a-3p, we also analyzed lncRNAs and mRNAs that might be associated with miR-328a-3p. The sequences of miR-328a-3p were highly conserved in different species, including human (*H. Sapiens*) and rats (*R. Norvegicus*). Considering that we have obtained the transcriptome profiles and identified ceRNA networks of rats after peripheral nerve injury (33), here, we determined lncRNA-miR-328a-3p-mRNA interactions, constructed a miR-328a-3p-centered ceRNA network, and explored the temporal expression patterns of miR-328a-3p-associated lncRNAs and mRNAs in the injured sciatic nerves of rats. Following peripheral nerve injury, the expression levels of miR-328a-3p first decreased, reaching a valley level at 4 days after nerve injury, and then gradually recovered to the uninjured level at 14 days (12). The heatmaps showed that inverse correlations were observed between the temporal expression profiles of miR-328a-3p and all predicted upstream lncRNAs as well as miR-328a-3p and potential target genes Vsig4 and Prdx5. Vsig4 encoded for a v-set and immunoglobulin-domain containing protein and was mainly considered as a negative regulator of T-cell responses (34, 35). Prdx5 encoded for peroxiredoxin 5, a member of the peroxiredoxin family of antioxidant enzymes, and played essential antioxidant roles (36). The involvements of Vsig4 and Prdx5 in the peripheral nervous system have not been clearly illuminated yet although Prdx5 was found to be expressed in peripheral nerves (37) and up-regulated in dorsal root ganglia neurons after peripheral nerve injury (38). Here, our sequencing data showed that the abundances of Vsig4 and Prdx5 were elevated in sciatic nerve stumps after nerve injury and elevated Vsig4 and Prdx5 might be induced by down-regulated miR-328a-3p. The binding relationships of lncRNAs and mRNAs with miR-328a-3p might be further validated by the luciferase assay and functional rescue assays.

Conclusions

Collectively, in the current study, we investigated the biological effects of miR-328a-3p and found that miR-328a-3p could encourage the migration and angiogenesis of endothelial cells. These findings provided certain cues for the regulation of endothelial cells during peripheral nerve regeneration.

Declarations

Availability of data and materials: The datasets used and analyzed during the current study are available from the corresponding author on reasonable request.

Competing interests: The authors declare that they have no conflict of interest.

Ethic approval and consent to participate: Experiments were ethically approved by the Administration Committee of Experimental Animals, Nantong University, Jiangsu Province, China and the Institutional Animal Care Guideline of Nantong University and complied with the Guide for the Care and Use of Laboratory Animals approved by the National Institutes of Health.

Consent for publication: Not applicable.

Availability of data and material: Data are available from the corresponding authors on reasonable request.

Authors' contributions: Conceived and designed the experiments: SY XW. Performed the experiments: SC YZ XC. Analyzed the data: SC XW. Contributed reagents/materials/analysis tools: SY XW. Wrote the manuscript: SY XW.

References

1. Eelen G, de Zeeuw P, Treps L, Harjes U, Wong BW, Carmeliet P. Endothelial Cell Metabolism. Physiol Rev. 2018;98(1):3-58.
2. Hassan M, Moghadamrad S, Sorribas M, Muntet SG, Kellmann P, Trentesaux C, et al. Paneth cells promote angiogenesis and regulate portal hypertension in response to microbial signals. J Hepatol. 2020;73(3):628-39.
3. Velazquez OC. Angiogenesis and vasculogenesis: inducing the growth of new blood vessels and wound healing by stimulation of bone marrow-derived progenitor cell mobilization and homing. J Vasc Surg. 2007;45 Suppl A:A39-47.

4. Rossi L, Attanasio C, Vilardi E, De Gregorio M, Netti PA. Vasculogenic potential evaluation of bottom-up, PCL scaffolds guiding early angiogenesis in tissue regeneration. Journal of materials science Materials in medicine. 2016;27(6):107.

5. Wong HK, Ivan Lam CR, Wen F, Mark Chong SK, Tan NS, Jerry C, et al. Novel method to improve vascularization of tissue engineered constructs with biodegradable fibers. Biofabrication. 2016;8(1):015004.

6. Lloyd-Griffith C, McFadden TM, Duffy GP, Unger RE, Kirkpatrick CJ, O'Brien FJ. The pre-vascularisation of a collagen-chondroitin sulphate scaffold using human amniotic fluid-derived stem cells to enhance and stabilise endothelial cell-mediated vessel formation. Acta biomaterialia. 2015;26:263-73.

7. Cattin AL, Burden JJ, Van Emmenis L, Mackenzie FE, Hoving JJ, Garcia Calavia N, et al. Macrophage-Induced Blood Vessels Guide Schwann Cell-Mediated Regeneration of Peripheral Nerves. Cell. 2015;162(5):1127-39.

8. Muangsanit P, Shipley RJ, Phillips JB. Vascularization Strategies for Peripheral Nerve Tissue Engineering. Anat Rec (Hoboken). 2018;301(10):1657-67.

9. Saffari TM, Bedar M, Hundepool CA, Bishop AT, Shin AY. The role of vascularization in nerve regeneration of nerve graft. Neural regeneration research. 2020;15(9):1573-9.

10. Ambros V. The functions of animal microRNAs. Nature. 2004;431(7006):350-5.

11. Bartel DP. MicroRNAs: genomics, biogenesis, mechanism, and function. Cell. 2004;116(2):281-97.

12. Yu B, Zhou S, Wang Y, Ding G, Ding F, Gu X. Profile of microRNAs following rat sciatic nerve injury by deep sequencing: implication for mechanisms of nerve regeneration. PLoS One. 2011;6(9):e24612.

13. Yu B, Zhou S, Yi S, Gu X. The regulatory roles of non-coding RNAs in nerve injury and regeneration. Progress in neurobiology. 2015;134:122-39.

14. Zou Y, Wu F, Liu Q, Deng X, Hai R, He X, et al. Downregulation of miRNA328 promotes the angiogenesis of HUVECs by regulating the PIM1 and AKT/mTOR signaling pathway under high glucose and low serum condition. Molecular medicine reports. 2020;22(2):895-905.

15. Oliverio M, Schmidt E, Mauer J, Baitzel C, Hansmeier N, Khani S, et al. Dicer1-miR-328-Bace1 signalling controls brown adipose tissue differentiation and function. Nature cell biology. 2016;18(3):328-36.

16. Yi W, Tu MJ, Liu Z, Zhang C, Batra N, Yu AX, et al. Bioengineered miR-328-3p modulates GLUT1-mediated glucose uptake and metabolism to exert synergistic antiproliferative effects with chemotherapeutics. Acta Pharm Sin B. 2020;10(1):159-70.

17. Eiring AM, Harb JG, Neviani P, Garton C, Oaks JJ, Spizzo R, et al. miR-328 functions as an RNA decoy to modulate hnRNP E2 regulation of mRNA translation in leukemic blasts. Cell. 2010;140(5):652-65.

18. Lu Y, Zhang Y, Wang N, Pan Z, Gao X, Zhang F, et al. MicroRNA-328 contributes to adverse electrical remodeling in atrial fibrillation. Circulation. 2010;122(23):2378-87.

19. Ruan ZB, Wang F, Bao TT, Yu QP, Chen GC, Zhu L. Genome-wide analysis of circular RNA expression profiles in patients with atrial fibrillation. International journal of clinical and experimental pathology. 2020;13(8):1933-50.

20. Guo W, Mu K, Zhang B, Sun C, Zhao L, Li HR, et al. The circular RNA circ-GRB10 participates in the molecular circuitry inhibiting human intervertebral disc degeneration. Cell death & disease. 2020;11(8):612.

21. Wei Y, Chen X, Liang C, Ling Y, Yang X, Ye X, et al. A Noncoding Regulatory RNAs Network Driven by Circ-CDYL Acts Specifically in the Early Stages Hepatocellular Carcinoma. Hepatology. 2020;71(1):130-47.

22. Saba R, Goodman CD, Huzarewich RL, Robertson C, Booth SA. A miRNA signature of prion induced neurodegeneration. PLoS One. 2008;3(11):e3652.

23. Zudaire E, Gambardella L, Kurcz C, Vermeren S. A computational tool for quantitative analysis of vascular networks. PLoS One. 2011;6(11):e27385.

24. Yi S, Zhang H, Gong L, Wu J, Zha G, Zhou S, et al. Deep Sequencing and Bioinformatic Analysis of Lesioned Sciatic Nerves after Crush Injury. PLoS One. 2015;10(12):e0143491.

25. Zhao L, Yi S. Transcriptional landscape of alternative splicing during peripheral nerve injury. Journal of cellular physiology. 2019;234(5):6876-85.

26. Roush S, Slack FJ. The let-7 family of microRNAs. Trends in cell biology. 2008;18(10):505-16.

27. Ji X, Hua H, Shen Y, Bu S, Yi S. Let-7d modulates the proliferation, migration, tubulogenesis of endothelial cells. Mol Cell Biochem. 2019;462(1-2):75-83.

28. Yan BL, Li XL, An JY. MicroRNA-328 acts as an anti-oncogene by targeting ABCG2 in gastric carcinoma. Eur Rev Med Pharmacol Sci. 2019;23(14):6148-59.

29. Shi J, An G, Guan Y, Wei T, Peng Z, Liang M, et al. miR-328-3p mediates the anti-tumor effect in osteosarcoma via directly targeting MMP-16. Cancer Cell Int. 2019;19:104.

30. Xiao B, Chen D, Zhou Q, Hang J, Zhang W, Kuang Z, et al. Glutamate metabotropic receptor 4 (GRM4) inhibits cell proliferation, migration and invasion in breast cancer and is regulated by miR-328-3p and miR-370-3p. BMC Cancer. 2019;19(1):891.

31. Qin X, Guo J. MicroRNA-328-3p Protects Vascular Endothelial Cells Against Oxidized Low-Density Lipoprotein Induced Injury via Targeting Forkhead Box Protein O4 (FOXO4) in Atherosclerosis. Med Sci Monit. 2020;26:e921877.

32. Smaila BD, Holland SD, Babaeijandaghi F, Henderson HG, Rossi FMV, Ramer MS. Systemic hypoxia mimicry enhances axonal regeneration and functional recovery following peripheral nerve injury. Experimental neurology. 2020;334:113436.

33. Qian T, Fan C, Liu Q, Yi S. Systemic functional enrichment and ceRNA network identification following peripheral nerve injury. Mol Brain. 2018;11(1):73.

34. Jung K, Seo SK, Choi I. Endogenous VSIG4 negatively regulates the helper T cell-mediated antibody response. Immunol Lett. 2015;165(2):78-83.

35. Vogt L, Schmitz N, Kurrer MO, Bauer M, Hinton HI, Behnke S, et al. VSIG4, a B7 family-related protein, is a negative regulator of T cell activation. The Journal of clinical investigation. 2006;116(10):2817-26.

36. Hanschmann EM, Godoy JR, Berndt C, Hudemann C, Lillig CH. Thioredoxins, glutaredoxins, and peroxiredoxins–molecular mechanisms and health significance: from cofactors to antioxidants to redox signaling. Antioxid Redox Signal. 2013;19(13):1539-605.

37. Lu JL, Vallat JM, Pollard JD, Knoops B, Ouvrier R. Expression of the antioxidant enzyme peroxiredoxin 5 in the human peripheral nervous system. J Peripher Nerv Syst. 2006;11(4):318-24.

38. Valek L, Kanngiesser M, Haussler A, Agarwal N, Lillig CH, Tegeder I. Redoxins in peripheral neurons after sciatic nerve injury. Free Radic Biol Med. 2015;89:581-92.

Figures
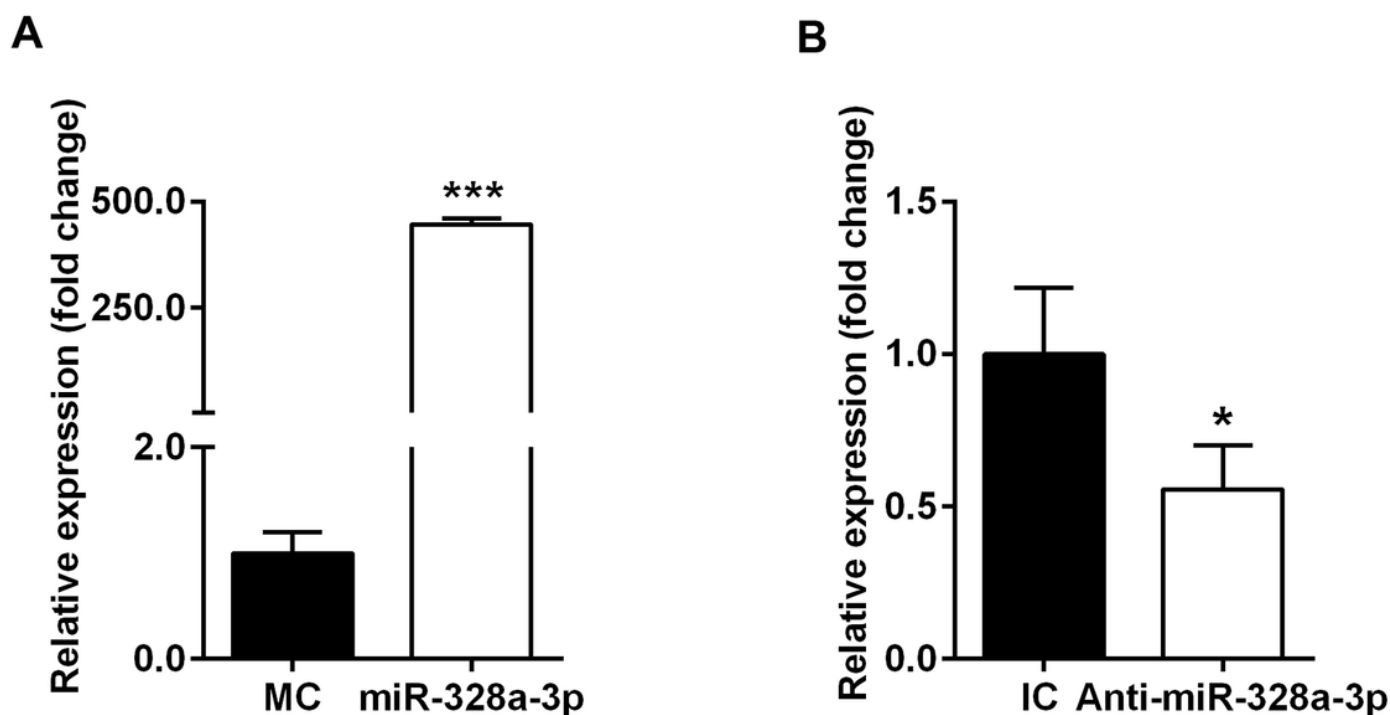
Figure 1

Transfection efficiency of miR-328a-3p mimic or inhibitor. (A) Transfection with miR-328a-3p mimic (miR-328a-3p), as compared with transfection with mimic control (MC), increased the relative abundance of miR-328a-3p. Summarized data were presented as mean with SEM from 3 experiments. ***, p-value<0.001. (B) Transfection with miR-328a-3p inhibitor (Anti-miR-328a-3p), as compared with transfection with inhibitor control (IC), decreased the relative abundance of miR-328a-3p. Summarized data were presented as mean with SEM from 3 experiments. *, p-value<0.05.
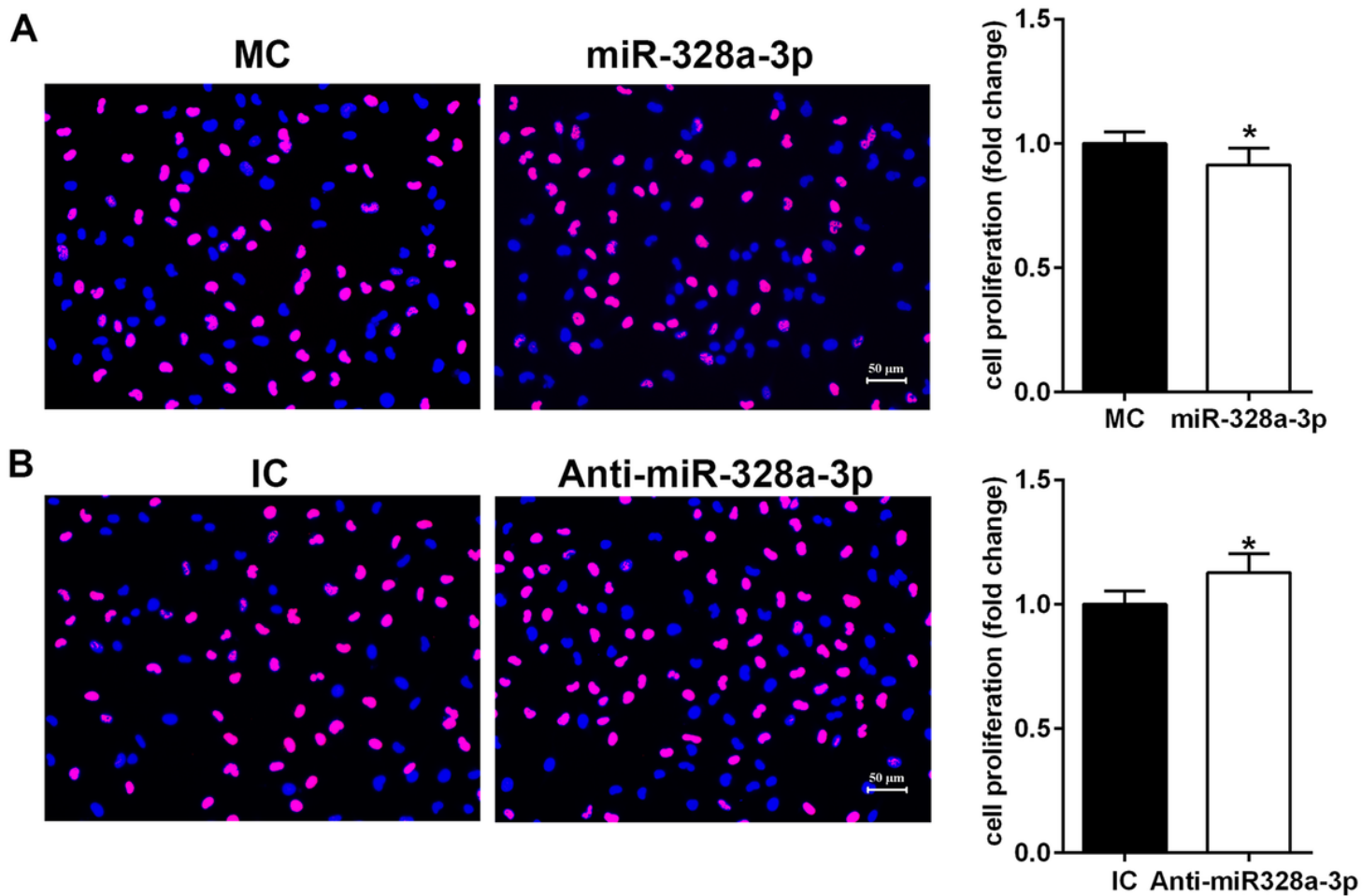
Figure 2

The effect of miR-328a-3p on HUVEC proliferation. (A) Transfection with miR-328a-3p mimic (miR-328a-3p), as compared with transfection with mimic control (MC), decreased cell proliferation rate. Red color indicated EdU staining while blue color indicated Hoechst 33342 staining. Scale bar: 50 μm. Summarized data were presented as mean with SEM from 4 experiments. *, p-value<0.05. (B) Transfection with miR-328a-3p inhibitor (Anti-miR-328a-3p), as compared with transfection with inhibitor control (IC), increased cell proliferation rate. Summarized data were presented as mean with SEM from 3 experiments. *, p-value<0.05.
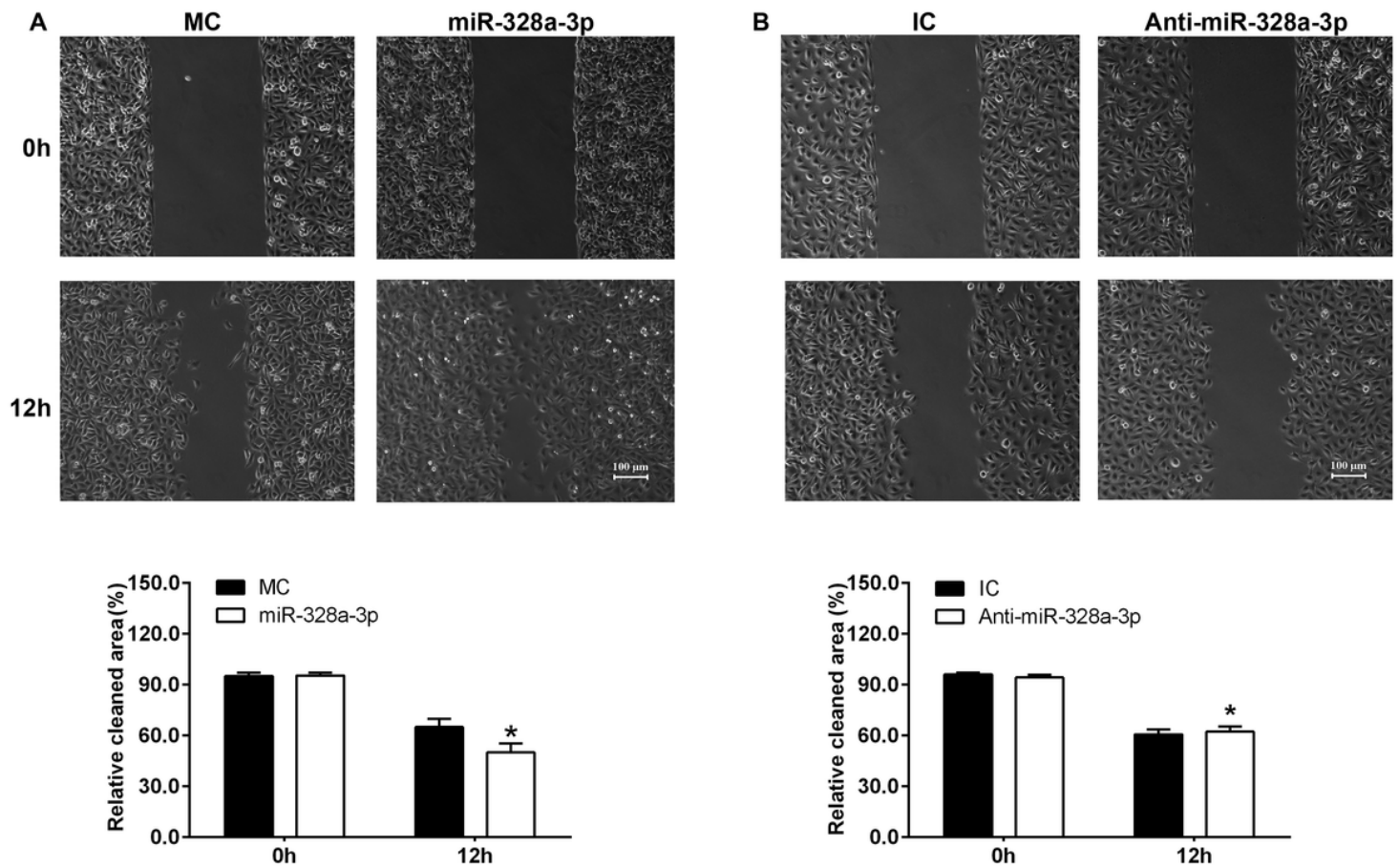
Figure 3

The effect of miR-328a-3p on HUVEC wound healing. (A) Transfection with miR-328a-3p mimic (miR-328a-3p), as compared with transfection with mimic control (MC), decreased relative cleaned area. Scale bar: 100 μm. Summarized data were presented as mean with SEM from 4 experiments. *, p-value<0.05. (B) Transfection with miR-328a-3p inhibitor (Anti-miR-328a-3p), as compared with transfection with inhibitor control (IC), increased relative cleaned area. Summarized data were presented as mean with SEM from 4 experiments. *, p-value<0.05.
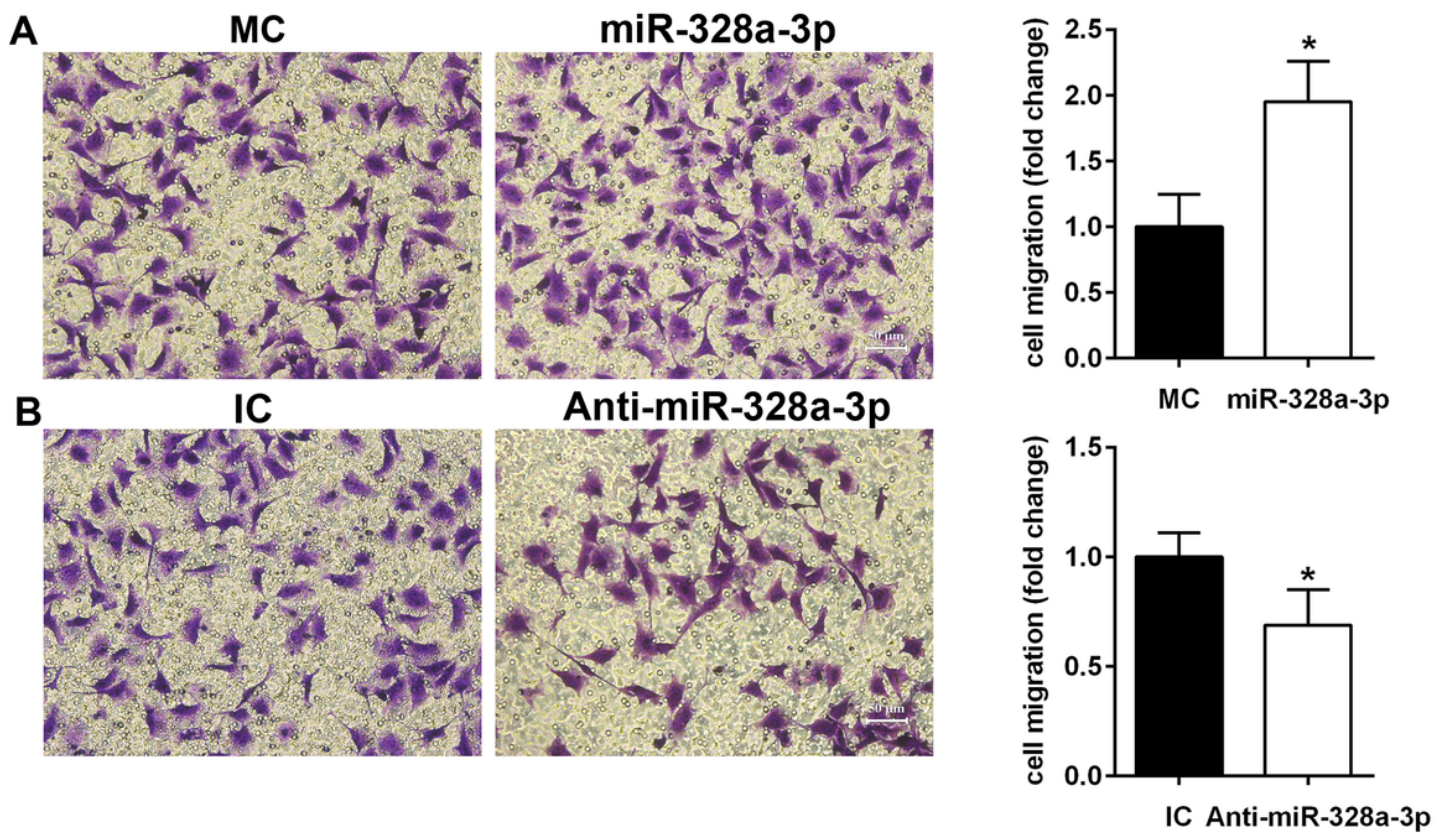
Figure 4

The effect of miR-328a-3p on HUVEC migration. (A) Transfection with miR-328a-3p mimic (miR-328a-3p), as compared with transfection with mimic control (MC), increased cell migration rate. Violet color indicated cells migrated through transwell chambers. Scale bar: 50 μm. Summarized data were presented as mean with SEM from 4 experiments. *, p-value<0.05. (B) Transfection with miR-328a-3p inhibitor (Anti-miR-328a-3p), as compared with transfection with inhibitor control (IC), decreased cell migration rate. Summarized data were presented as mean with SEM from 3 experiments. *, p-value<0.05.
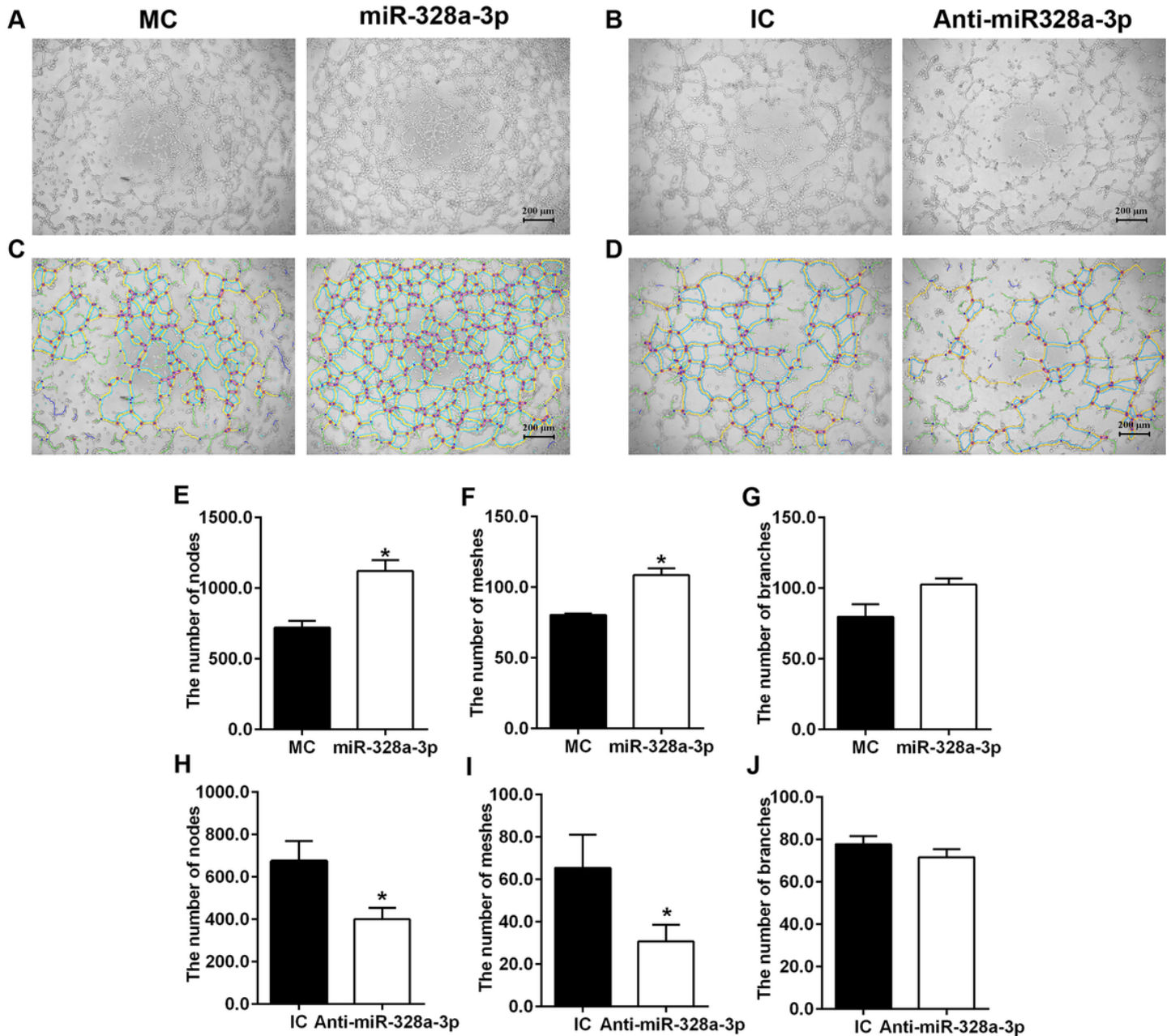
Figure 5

The effect of miR-328a-3p on HUVEC tubulogenesis. (A) Transfection with miR-328a-3p mimic (miR-328a-3p), as compared with transfection with mimic control (MC), increased cell tubulogenesis. Scale bar: 200 μm. (B) Transfection with miR-328a-3p inhibitor (Anti-miR-328a-3p), as compared with transfection with inhibitor control (IC), decreased cell tubulogenesis. (C, D) Skeletonized images of capillary-like tubes formed by HUVECs transfected with (C) miR-328a-3p mimic or mimic control and (D) miR-328a-3p inhibitor or inhibitor control. (E) The number of nodes in HUVEC transfected with miR-328a-3p mimic or mimic control. Data were presented as mean with SEM from 4 experiments. *, p-value<0.05. (F) The number of meshes in HUVEC transfected with miR-328a-3p mimic or mimic control. Data were presented as mean with SEM from 3 experiments. *, p-value<0.05. (G) The number of branches in HUVEC transfected with miR-328a-3p mimic or mimic control. Data were presented as mean with SEM from 4

experiments. *, p-value<0.05. (H) The number of nodes in HUVEC transfected with miR-328a-3p inhibitor or inhibitor control. Data were presented as mean with SEM from 4 experiments. *, p-value<0.05. (I) The number of meshes in HUVEC transfected with miR-328a-3p inhibitor or inhibitor control. Data were presented as mean with SEM from 4 experiments. *, p-value<0.05. (J) The number of branches in HUVEC transfected with miR-328a-3p inhibitor or inhibitor control. Data were presented as mean with SEM from 4 experiments. *, p-value<0.05.
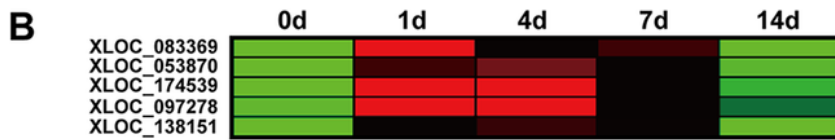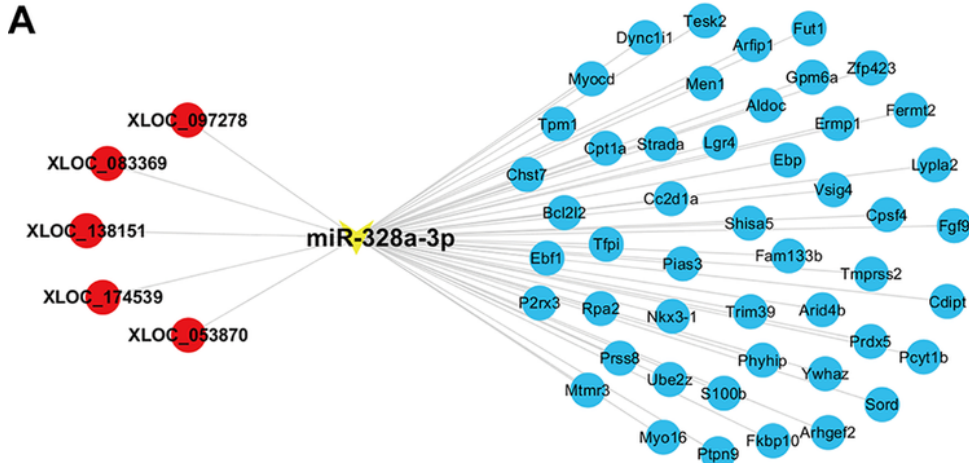
Figure 6

The ceRNA network of miR-328a-3p. (A) Interactions of lncRNAs, miR-328a-3p, and target mRNAs in the miR-328a-3p-centered ceRNA network. lncRNAs were labeled in red color, miRNA was labeled in yellow color, and mRNAs were labeled in blue color. (B) Heatmap of the temporal expression patterns of lncRNAs in the miR-328a-3p-centered ceRNA network in the sciatic nerve stumps at 0, 1, 4, 7, and 14 days after nerve crush injury. Red color indicated up-regulation while green color indicated down-regulation. (C) Heatmap of the temporal expression patterns of mRNAs in the miR-328a-3p-centered ceRNA network in the sciatic nerve stumps at 0, 1, 4, 7, and 14 days after nerve crush injury.